Journal of Applied Polymer Science

In Vitro Silver Ion Release Kinetics from Nanosilver/Poly(vinyl alcohol) Hydrogels Synthesized by Gamma Irradiation

Jelena Krstić,[1] Jelena Spasojević,[1] Aleksandra Radosavljević,[1] Aleksandra Perić-Grujić,[2] Momčilo Đurić,[3] Zorica Kačarević-Popović,[1] Srđan Popović[4]

[1]Vinča Institute of Nuclear Sciences, University of Belgrade, P.O. Box 522, Belgrade 11001, Serbia

[2]Faculty of Technology and Metallurgy, University of Belgrade, P.O. Box 35-08, Belgrade 11120, Serbia

[3]Institute of Microbiology, Military Medical Academy, P.O. Box 33-55, Belgrade 11040, Serbia

[4]Clinic for Endocrinology, Diabetes, and Metabolic Diseases, Faculty of Medicine, University of Belgrade, P. O. Box 497, Belgrade 11000, Serbia

Correspondence to: A. Kačarević-Popović (E-mail: zkacar@vinca.rs) or S. Popović (E-mail: prof.srdjan.popovic@gmail.com)

ABSTRACT: A nanosilver (nano-Ag)/poly(vinyl alcohol) (PVA) hydrogel device was synthesized with γ irradiation because it is a highly suitable tool for enhanced nano-Ag technologies and biocompatible controlled release formulations. The amount of the Ag^+ ions released *in vitro* by the nano-Ag/PVA hydrogel device was in the antimicrobial parts per million concentration range. The modeling of the Ag^+ ion release kinetics with the elements of the drug-delivery paradigm revealed the best fit solution ($R^2 > 0.99$) for the Kopcha and Makoid–Banakar's pharmacokinetic dissolution models. The term A/B, derived from the Kopcha model, indicated that the nano-Ag/PVA hydrogel was mainly an Ag^+-ion diffusion-controlled device. Makoid–Banakar's parameter and the short time approximated Ag^+-ion diffusion constant reflected the importance of the size of the Ag nanoparticles. However, it appeared that the cell oxidation potential of the Ag nanoparticles depended on the diffusion characteristics of the fluid penetrating into the Ag/PVA nanosystem. © 2014 Wiley Periodicals, Inc. J. Appl. Polym. Sci. **2014**, *131*, 40321.

KEYWORDS: composites; drug-delivery systems; hydrophilic polymers; gels; irradiation

Received 23 August 2013; accepted 17 December 2013

DOI: 10.1002/app.40321

INTRODUCTION

Hydrogels are hydrophilic bicomponent or multicomponent systems consisting of three-dimensional networks of polymer chains and liquid that fills the space between macromolecules. Because they have the possibility of absorbing large amounts of water and biological fluids, they are biocompatible, and therefore, they are often used in patient care and wound dressings.[1] Hydrogels facilitate autolysis and may be beneficial in the management of ulcers containing necrotic tissue. For example, debridement with hydrogels is more effective than standard wound care for healing diabetic foot ulcers.[2] A potential problem for the biomedical application of hydrogels is that microorganisms may grow in hydrogel materials because of their natural biocompatible properties. Therefore, the incorporation of antibacterial agents is required. However, the emergence of antibiotic-resistant bacteria as a result of the excessive use of antibiotics has led to a demand for newer antimicrobials. It is especially important for patients with diabetes because they are more prone to infections, as they have reduced leukocyte activity, decreased phagocytosis, poor bactericidal activity, and a buildup of debris.[2]

The increasing need to develop new formulations to solve this problem has led to considerable interest in the use of nanomaterials as new types of antimicrobials. Nanosilver (nano-Ag) has been proven to be the most effective antimicrobial agent.[3–7] The multilevel antimicrobial mode of Ag is particularly important for the treatment of wound infections in diabetic patients, which are usually polymicrobial, with the majority of infections being caused by aerobic Gram-positive cocci (predominantly *Staphylococcus aureus* and hemolytic *Streptococci*).[8,9]

Recent studies have suggested that Ag nanoparticles exert toxicity on bacteria and other organisms not by direct particle-specific effect but by released Ag^+ ions.[10] Ag^+ ions might interact with the S—H bounds of the proteins, and this leads to their inactivation. When the pathways in the antibacterial activity and eukaryotic toxicity of Ag nanoparticles involve the Ag^+ ions and their soluble complexes, Ag nanoparticles behave like a drug-delivery system, in which the particles contain a concentrated inventory of active species, the ions.[11] Although the importance of Ag^+ ions in the biological response to Ag nanoparticles is widely recognized, the drug-delivery paradigm has

not been well developed for this system,[11] and therefore, there is significant potential to improve nano-Ag technologies through hydrogel controlled release formulations. However, to find application in the biomaterials field, both stabilizing hydrogels and reducing agents for nanoparticle synthesis must not represent a biological hazard. Poly(vinyl alcohol) (PVA) is already used in biomedical application for wound dressings; they show better wound cleaning and a more rapid growth compared with other materials.[12] However, the toxicity of glutaraldehyde and hexamethylene diisocyanate, probably the most known crosslinking agents of PVA-based chemical hydrogels, can substantially affect the biocompatibility of the resulting material. This problem can be solved with the method of radiolytic crosslinking, because this process takes place without substances such as crosslinkers and initiators, which are possibly harmful and difficult to remove.[13,14] In addition, ionizing irradiation is very suitable for the generation of noble-metal nanoparticles within the polymer network of hydrogels.[15–18] Even though the chemical methods for synthesis of nanoparticles involve a very simple procedure, they use chemical reducing agents, such as citrate, borohydride, or other organic compounds, that are toxic to living organisms. This makes them unsuitable for medical use. Solvated electrons and secondary radicals, formed by the radiolysis of water, have significant reduction power and the ability to convert silver ions (Ag^+) to their atomic state.[19–21]

Moreover, for the use of nano-Ag-loaded hydrogels in biomedicine, it should be possible to modulate the release of Ag^+ ions, which could be delivered to the patient at a controlled rate. This would allow the achievement of adequate concentrations and prolonged effectiveness. Thus, in this study, we aimed to quantify the amount of Ag^+ ions released in an *in vitro* medium and to use for the first time the elements of the pharmacokinetic drug-delivery paradigm to the nano-Ag/PVA hydrogel as a model system for the evaluation of the release kinetics and the release mechanism. This was contrary to previous studies, which were mainly based on the development of hydrogel systems as a templates for the synthesis of nanoparticles.[22–30] In general, it is known that the release of a soluble drug entrapped in a hydrogel should be closely related to the swelling characteristics of the hydrogels. That is because the release occurs only after the fluid penetrates into the polymeric network and dissolves the drug; this is followed by diffusion along the aqueous pathways to the surface of the device.[31] Therefore, the swelling characteristics of a nano-Ag/PVA hydrogel device and the diffusion parameters of simulated body fluid (SBF; at 37°C) were investigated. Finally, antibacterial assessment was performed toward Gram-positive *S. aureus* and Gram-negative *Escherichia coli*.

EXPERIMENTAL

Materials

All chemicals were commercial products of analytical grade and were used without further purification. PVA (with a weight-average molecular weight of 72 kDa and a 99% minimal degree of hydrolysis), silver nitrate ($AgNO_3$), 2-propanol [$(CH_3)_2CHOH$], potassium chloride (KCl), calcium chloride dihydrate ($CaCl_2 \times 2H_2O$), and tris(hydroxymethyl)aminomethane [$(CH_2OH)_3CNH_2$] were supplied from Merck (Germany). Potassium dihydrogen phosphate (KH_2PO_4) and potassium hydrogen phosphate (K_2HPO_4) were obtained from Kemika (Croatia). Sodium chloride (NaCl), sodium sulfate (Na_2SO_4), and sodium hydrogen carbonate ($NaHCO_3$) were obtained from Zorka Pharma (Serbia). Magnesium chloride dihydrate ($MgCl_2 \times 2H_2O$) was obtained from Centrohem (Serbia). Hydrochloric acid (HCl) and nitric acid (HNO_3) were obtained from J. T. Baker. Solutions were prepared with water obtained with a Milli-Q water system (Millipore Corp.), which had a purity that was four times that of distilled water. Before γ irradiation, the solutions were saturated with argon gas (Ar; Messer Tehnogas, Serbia) with a high purity (99.5%). All of the systems were exposed to γ rays (^{60}Co source) in closed cells under ambient conditions.

Synthesis of the Nano-Ag/PVA Hydrogel Device

Synthesis of the PVA Hydrogel. A volume of 40 mL of the PVA solution (5% w/w) was obtained by the dissolution of PVA in distilled water at 90°C for 3 h with constant mixing. To remove oxygen, the polymer solution was bubbled with argon for 20 min and then poured into specially designed molds. The molds consisted of two glass plates, which were mutually separated by rubber spacers. The filled molds were exposed to γ irradiation to induce crosslinking at a dose rate of 0.33 kGy/h up to an absorbed dose of 25 kGy. The obtained hydrogel was extracted in distilled water for 7 days (with the water changed daily) to remove the residual noncrosslinked polymer chains. The mass yield of the hydrogel (W) was 90%, and it was obtained by a previously reported procedure,[17] according to the following expression:

$$W(\%) = \frac{W_g}{W_0} \times 100 \quad (1)$$

where W_g is the weight of the xerogel after extraction and W_0 is the initial weight of the polymer.

***In Situ* Synthesis of the Ag Nanoparticles in the PVA Hydrogel.** After the irradiation-induced crosslinking and extraction processes, the PVA hydrogel samples [disk diameter = 10 mm, thickness = 4 mm] were dried. Then, the samples of the obtained PVA xerogel (dried gel) were left to swell in solutions (20 mL) containing different concentrations of $AgNO_3$ (4, 8, 16, 30, 75, and 100 mM) and 0.2M 2-propanol, which were previously saturated with argon to remove oxygen. The swelling of the samples was carried out in sealed cells at room temperature in the dark for 48 h [the time needed to reach the equilibrium swelling degree (SD_{eq})]. These samples were exposed to γ irradiation (at a dose rate of 10 kGy/h) up to 7, 14, 28, 53, 133, and 177 kGy, respectively, to perform a reduction of Ag^+ ions in the hydrogels. The obtained hydrogel nanocomposites (HG NCs) were labeled S1, S2, S3, S4, S5, and S6, and the pure PVA hydrogel was labeled S7. After irradiation, the characteristic yellow nano-Ag/PVA hydrogels were observed.

Methods of Characterization. ***Optical and structural characterization.*** Ultraviolet–visible (UV–vis) absorption spectra of the hydrogels, PVA, and nano-Ag/PVA hydrogel were recorded with a Thermo Fisher Scientific Evolution 600 UV–vis

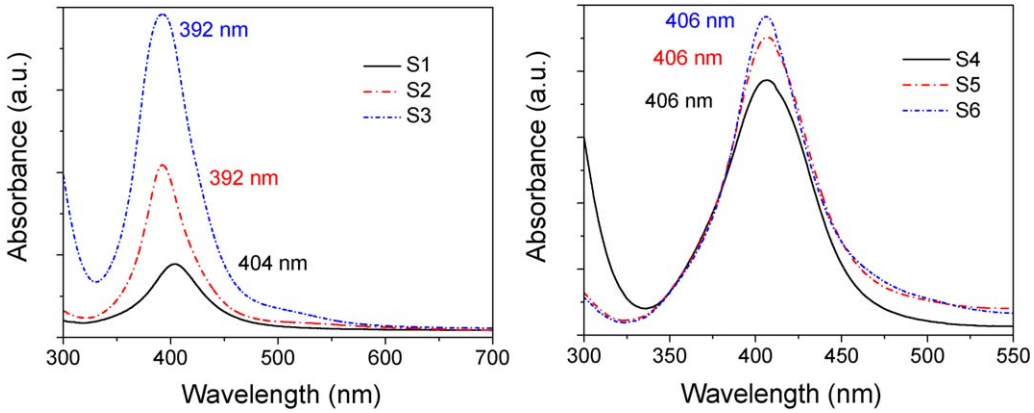

Figure 1. UV–vis absorption spectra of nano-Ag/PVA HG NCs devices with different molar concentrations, *Cs* of Ag nanoparticles. [Color figure can be viewed in the online issue, which is available at wileyonlinelibrary.com.]

spectrophotometer in the wavelength (λ) range 300–800 nm. The X-ray diffraction (XRD) and Fourier transform infrared (FTIR) measurements were performed on a Bruker D8 Advance diffractometer (Cu Kα radiation, $\lambda = 0.1541$ nm) and with a Thermo Electron Corp. Nicolet 380 spectrophotometer (working in attenuated total reflection mode), respectively.

Swelling studies. The swelling behaviors of the hydrogels, PVA, and nano-Ag/PVA hydrogel device were investigated in an excess of SBF at 37 ± 1°C. The SBF (pH = 7.4) was prepared according to the procedure for Kokubo's solution.[32] Xerogel discs (diameter = 3.83 ± 0.18 mm, thickness = 1.37 ± 0.13 mm) were immersed in SBF, and the process of swelling was monitored gravimetrically through the measurement of the weight of the swollen hydrogel (W_t) at predetermined time intervals until the initial weights were equilibrated. All of the experiments were performed in triplicate.

Ag^+ ion release investigation. The release of Ag^+ ions from the nano-Ag/PVA hydrogel device was examined at 37 ± 1°C in phosphate buffer (pH = 7) containing 0.039*M* KH_2PO_4 and 0.061*M* K_2HPO_4. Nano-Ag/PVA xerogel discs (diameter = 4.43 ± 0.19 mm, thickness = 1.31 ± 0.08 mm) were immersed in 10 mL of phosphate buffer, which was changed periodically after 1, 3, 5, 7, and 9 days. The release media were replaced per iodically with an equal volume of fresh solution to create infinite sink conditions. A Philips PYU UNICAM SP9 atomic absor ption spectrometer was used to measure the Ag^+ ions released from the samples. In addition, the total content of silver within the nano-Ag/PVA hydrogel device was determined upon treatment in HNO_3 (1:1 v/v) to induce the oxidation of all of the Ag nanoparticles into Ag^+ ions. The data represent the mean of three independent experiments.

Antimicrobial activity. The antibacterial properties of the Ag/PVA HG NCs were assessed with the agar diffusion test. Petri dishes covered with solidified nutrition agar base (2% agar) were inoculated with *E. coli* (ATTC 25922) and *S. aureus* (ATTC 25923) inside the layer of the top agar (0.7% agar). A volume of 20 mL of 18-h-old *E. coli* and *S. aureus* culture was added to 15 mL of the top agar solution and was put onto the nutritional agar base. After the solidification of the top agar layer, nano-Ag/PVA hydrogel discs (diameter ≤ 6 mm, thickness = 4 mm) were put in the Petri dishes and were then incubated at 37°C for 24 h. The samples with higher initial concentrations of Ag (S4, S5, and S6) were investigated after 2 weeks and 2 months of aging in buffered solution at room temperature, that is, after the smaller and larger losses of silver. The achievement of inhibitory concentrations of the released silver was observed as the absence of microbial growth, which could be seen as a clear zone around the disc specimens.

RESULTS AND DISCUSSION

The radiolytic method, as highly suitable tool for the crosslinking of polymers and the synthesis of Ag nanoparticles within the polymeric network of hydrogels, is based on the process of the radiolysis of water, which induces the formation of several primary products [hydrated electrons (e_{aq}^-), H_3O^+ ions, hydroxyl and hydrogen radicals ($OH^\bullet$ and $H^\bullet$), etc.]. $OH^\bullet$ radicals participate in the process of the crosslinking of PVA, whereas e_{aq}^-, 2-propanol radicals [$(CH_3)_2C^\bullet OH$], and $PVA^\bullet$ allow the reduction of Ag^+ ions and the formation of Ag nanoparticles.[18–21]

Optical and Structural Properties

The obtained UV–vis absorption spectra (Figure 1) of the nano-Ag/PVA hydrogel device showed the surface plasmon bands peaking in the range 392–406 nm because of the formation of Ag nanoparticles.[16–18]

When the sizes of the metal nanoparticles were smaller than the λ of incident light, their average radius (r) values could be estimated from the surface plasmon resonance band with the following expression:[33,34]

$$r = \frac{v_f}{\Delta\omega_{1/2}} \quad (2)$$

where v_f is the Fermi velocity for Ag (1.39×10^8 m/s) and $\Delta\omega_{1/2}$ is the full width at half-maximum in units of angular frequency for the surface plasmon resonance band of the nanoparticles. This relation assumes that the particles are spherical, without any interparticle interaction.[34]

The Ag nanoparticles' r values are given in Table I. The r obtained for sample S2 was the smallest, probably because a better balance between the adsorption energy per monomer at

Table I. Calculated Values of r, C,[a] Theoretical SA, and S_r of the Ag Nanoparticles in the PVA Hydrogel

Sample	$C_{AAS} \times 10^6$ (g/cm^3)	fwhm (nm)	r (nm)	$C_{HG\ NC} \times 10^{11}$ (mol/cm^3)	SA of NPs (m^2/g)	S_r (mg/L)
S1	117.2	55.90	4.12	6.31	69.3	0.067
S2	97.2	44.67	3.30	10.13	86.7	0.111
S3	201.1	54.25	4.00	11.79	71.4	0.071
S4	2169.4	56.99	4.20	110.41	67.9	0.065
S5	5409.7	56.99	4.20	275.63	67.9	0.065
S6	5524.5	49.87	3.68	419.26	77.6	0.086

fwhm, full width at half-maximum.
[a] C_{AAS} initial concentration of Ag doped in the hydrogel was obtained by atomic absorption measurements. $C_{HG\ NC}$ molar concentration of nanoparticles was calculated with eq. (3).

contact with the metal surface, polymer–solvent mixing energy, and configurational entropy loss due to chain confinement on the surface of the nanoparticles during the polymer adsorption process were achieved for sample S2, and this resulted in smaller nanoparticles.[35]

The crystalline structure and crystalline domain size of the Ag nanoparticles were estimated by XRD measurement. The obtained patterns are presented in Figure 2. The XRD peaks exactly matched the (111), (200), and (220) crystal planes of Ag with a face-centered cubic crystal structure.[17] The Scherrer diffraction formula was used to estimate the crystalline domain size (CD):

$$\mathrm{CD} = \frac{k\lambda}{\beta \cos\theta} \tag{3}$$

where $k = 0.9$ is a kinetic constant for the cubic structure, $\lambda = 0.1541$ nm, β is the peak angular width, and θ is the diffraction angle. The crystalline domain size was around 9 nm. This confirmed that the nanoparticles spanned intrinsic size ranges ($r = 1$–10 nm). Therefore, the quasi-static approximation of Mie theory held, and eq. (1) and UV–vis spectroscopy as a sizing technique[36–38] could be applied for the calculation of the nanoparticles' r values.

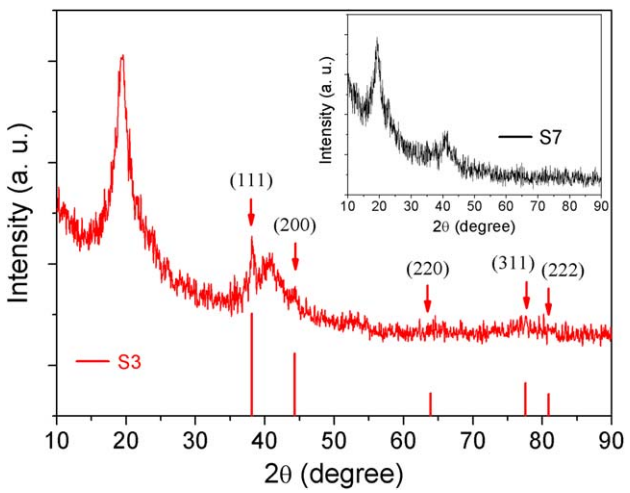

Figure 2. XRD patterns of the xerogels: nano-Ag/PVA (S3) and PVA (S7; insert). [Color figure can be viewed in the online issue, which is available at wileyonlinelibrary.com.]

In addition to the accurate determination of the size, the determination of the concentration of nanoparticles is essential for their biomedical application. With the assumption of the Ag bulk density (5.86×10^{22} atoms/cm^3), it was possible to determine the average number of Ag atoms belonging to spherical nanoclusters in the metallic phase (N), the cluster density in the sample (by the division of the total amount of Ag atoms, i.e., the initial amount of Ag^+ ions doped in samples and obtained by the atomic absorption measurements, by the average number of atoms in each particle), and finally, their molar concentration (C),[39] as shown in Table I:

$$C = \frac{N_{\mathrm{total}}}{NVN_A} \tag{4}$$

were N_{total} is equivalent to the initial amount of Ag^+ ions doped in the hydrogel sample, V is the volume of the reaction solution (hydrogel sample) and N_A is Avogadro's constant. It was assumed that the reduction from Ag^+ ions to Ag atoms was 100% complete.

Investigations have shown that many properties and applications of nanocrystals are surface-related and size-dependent because small nanoparticles have a greater fraction of atoms at the edges and corners than large particles, and this makes the surface more reactive. Therefore, in this study, the values obtained for r were used to calculate the theoretical surface area (SA) with the following equation:[40]

$$\mathrm{SA} = \frac{6}{2r \times \rho} \tag{5}$$

where $2r$ is the particle diameter and ρ is the theoretical density of Ag. The obtained results are given in Table I.

Finally, a modified form of the Kelvin equation (Ostwald–Freundlich relation) was used to relate the particle solubility to its r [eq. (5)]:[41,42]

$$S_r = S_{\mathrm{bulk}} \times \exp\left(\frac{2\gamma V_m}{RT} r\right) \tag{6}$$

where S_r is the solubility of Ag nanoparticles with r, S_{bulk} is the solubility of silver with a flat surface, γ is the surface tension of the particles (J/m^2), V_m is the molar volume of the particles (m^3/mol), R is the gas constant, and T is the temperature (K). The solubility parameters of the Ag nanoparticles are presented in Table I. As shown in Table I, the solubility of the nanoparticles was greater for the smaller particles.

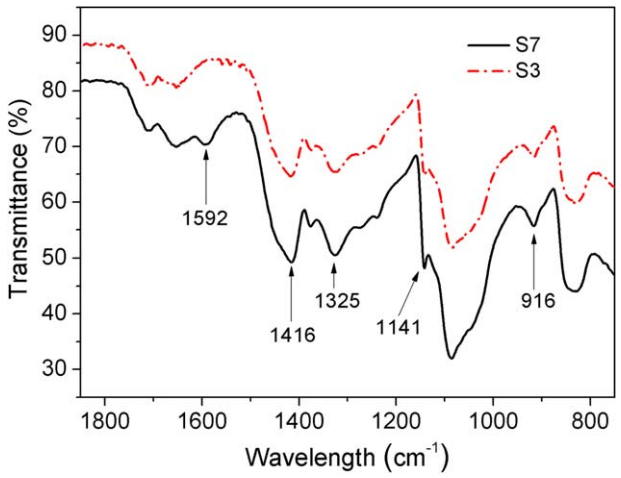

Figure 3. FTIR spectra of the pure PVA (S7) and nano-Ag/PVA xerogel nanocomposites (S3). [Color figure can be viewed in the online issue, which is available at wileyonlinelibrary.com.]

To obtain the molecular structure of the nano-Ag/PVA hydrogel device after the reduction of Ag^+ ions during the radiolytic synthesis of Ag nanoparticles, the FTIR spectra of xerogel samples were recorded. The obtained spectra confirmed that the stabilization of Ag nanoparticles took place over the interaction between the surface of the nanoparticles and the OH groups of the PVA chains, as shown in Figure 3. Namely, a decrease in the intensity of the band peaking at 1325 cm^{-1} (the result of the coupling of O—H in plane vibration) compared to the C—H wagging vibrations (the strong line at 1420 cm^{-1}) with increasing C of the Ag nanoparticles, indicated decoupling between the corresponding vibrations and interaction of Ag nanoparticles with the OH groups. This was in accordance with our previous study of radiolytically synthesized Ag/PVA HG NCs.[17] Because of this interaction, the bending and out-of-plane oscillations of the —OH groups of PVA were restricted. This, in turn, affected the chain mobility of PVA and also acted as physical crosslinks.[43] In addition, the disappearance of the band positioned around 1592 cm^{-1}, which was the result of β-diketone in residual vinyl acetate groups in partially hydrolyzed PVA,[44] was probably the consequence of interaction with Ag nanoparticles. The band at 1141 cm^{-1} corresponded to a symmetric C—C stretching mode in the ordered/crystalline regions of the PVA matrix. The presence of peaks at 916 cm^{-1} in all of the samples revealed the existence of a syndiotactic structure in the polymer chains.

Swelling Properties

The obtained time dependences of the swelling degree (SD) values for the pure PVA and nano-Ag/poly(vinyl alcohol) hydrogel device are depicted in Figure 4(a), where SD was calculated from the gravimetrically obtained swelling parameters by the following equation:[45]

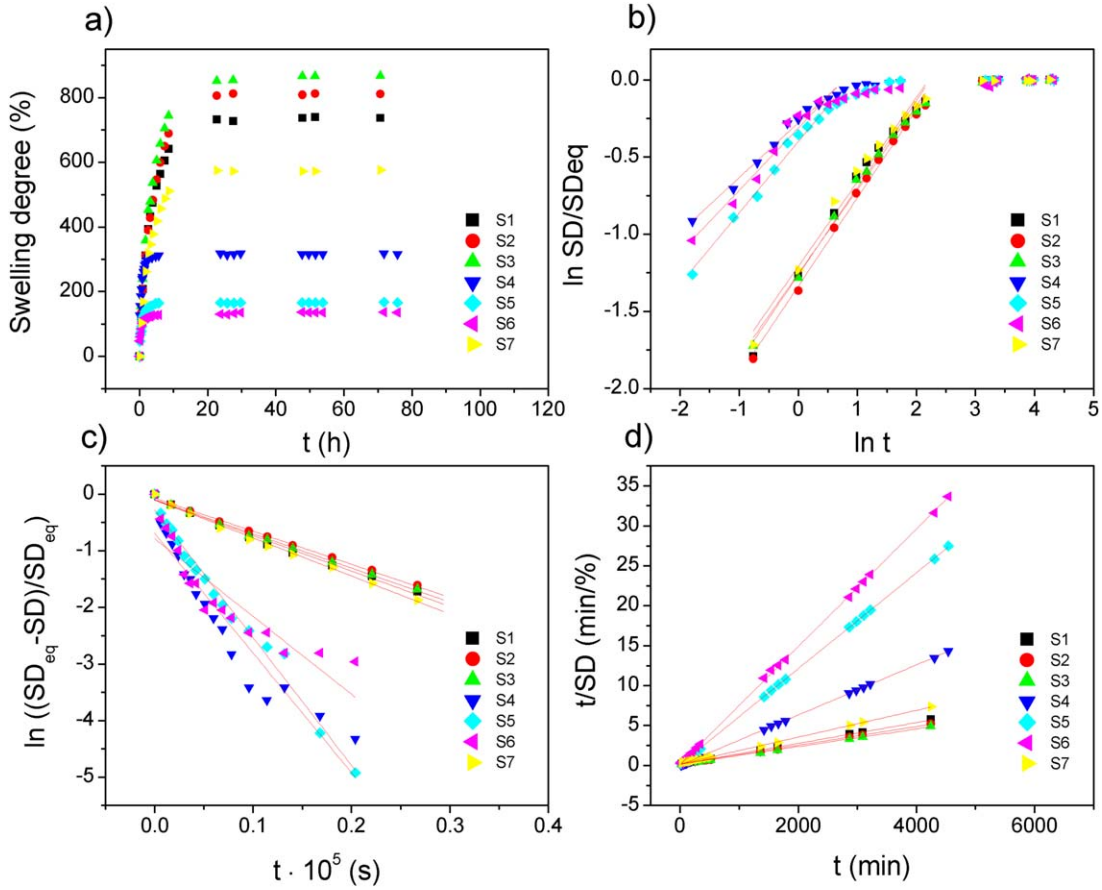

Figure 4. (a) Swelling curves of the PVA hydrogel and the nano-Ag/PVA hydrogel device, (b) power-law kinetics, (c) first-order kinetics, and (d) second-order kinetics in an SBF solution at 37°C (t is the time of swelling). [Color figure can be viewed in the online issue, which is available at wileyonlinelibrary.com.]

Table II. Values of SD_{eq}, k, and n for the Power Law Model, First-Order Kinetics, and Second-Order Kinetics

		Power law kinetics			First-order kinetics			Second-order kinetics		
Sample	SD_{eq} exp (%)	k_s (1/h^n)	n	R^2	Calculated SD_{eq} (%)	$k_{F\text{-}O} \times 10^4$ (1/s)	R^2	Calculated SD_{eq} (%)	v_0 (%/min)	R^2
S1	737	0.283	0.56	0.98	654	0.63	0.99	769	5.74	0.99
S2	811	0.263	0.57	0.99	730	0.59	0.99	855	5.42	0.99
S3	867	0.285	0.54	0.99	766	0.60	0.99	909	6.37	0.99
S4	317	0.758	0.35	0.98	300	2.12	0.90	318	5.14	0.99
S5	165	0.671	0.46	0.99	155	2.26	0.98	167	7.79	0.99
S6	135	0.733	0.40	0.96	123	1.38	0.79	136	5.91	0.99
S7	576	0.299	0.55	0.98	518	0.67	0.99	595	4.97	0.99

v_0 is the initial swelling rate and k_{F-O} is the first-order kinetic constant.

$$SD = \frac{W_t - W_0}{W_0} \quad (7)$$

where W_0 is the initial weight of the xerogel.

In addition, SD_{eq} was determined by the same equation, but we obtained the weight of the hydrogel in the equilibrium state (W_{eq}) instead of W_t at predetermined time intervals. The swelling equilibrium occurred when the values of the osmotic force driving the solvent into the network and the elastic force of the stretched subchains became equal.[46]

The swelling of the PVA and nano-Ag/PVA hydrogel device increased over time and reached constant values (equilibrium swelling) after about 30 h (Table II). The isothermal swelling capacity was higher for the nano-Ag/PVA hydrogel device (samples S1, S2, and S3) compared to that obtained for the PVA hydrogel (S7). Similar behavior was observed previously for radiolytically synthesized Ag/poly(vinyl pyrrolidone) HG NCs.[14,16] This property is important in the biomedical application of nanocomposite hydrogels for wound dressing applications because, compared to a pure hydrogel, Ag HG NCs can further absorb slight to moderate amounts of wound exudate by swelling. This helps in the rapid healing of certain types of wounds. An increase in the absorption of the surrounding fluid by a nano-Ag/PVA hydrogel device is probably caused by the presence of some amounts of dissolved Ag^+ ions. This changes the composition of the medium and the chemical environment of the network.[47,48] In addition, dissolved Ag^+ ions can generate an osmotic gradient,[49] which may result in a greater rate of polymer swelling.[50,51] On the other hand, for higher C values of the Ag nanoparticles (samples S4, S5, and S6), the swelling capacity decreased compared to that of the pure PVA hydrogel. This was probably caused by the restriction of the larger scale segmental motion of the polymer chains.

Kinetic Aspects and Diffusion Model of the Swelling Process. In this study, a power law approach was used to calculate the kinetic parameters of diffusion:[52,53]

$$\frac{SD}{SD_{eq}} = kt^n \quad (8)$$

where SD and SD_{eq} are the swelling degree at predetermined time intervals and at equilibrium, respectively; k is the kinetic constant related to the structure of the network and the penetran; t is the time and n is the diffusion exponent. To determine the diffusion model, eq. (8) was applied in the initial stage of swelling ($SD/SD_{eq} \leq 0.6$), where a linear trend of the data was observed. The values of the kinetic parameters k and n were determined from the curves of $\ln(SD/SD_{eq})$ versus $\ln t$ by linear fitting at the initial stage of swelling, as illustrated in Figure 4(b).

As shown clearly in Table II, at the initial stage of swelling, the systems showed non-Fickian diffusion ($0.5 < n < 1$) for both PVA (sample S7) and the nano-Ag/PVA hydrogel device (samples S1, S2, and S3); this meant that both diffusion and polymer relaxation processes controlled the fluid transport.[14,45,54] Moreover, the results show that parameter n was nearly constant for samples S1, S2, and S3 and for the pure PVA hydrogel (sample S7). Samples S4, S5, and S6 showed Fickian diffusion ($n < 0.5$). In this case, media transport was driven by a concentration gradient rather than by convective flux and was not severely limited by the relaxation of the polymer.[53] The kinetic constants (k_s; power low model), for samples S1, S2, and S3 were nearly constant. This indicated that the structure of the network did not change (crosslinked or degraded) and that the energy of irradiation applied for Ag nanoparticle synthesis was mostly spent on reduction of Ag^+ ions. For samples S4, S5, and S6, the values of s and k_{F-O} were greater compared to that of the pure PVA hydrogel (sample S7); this indicated that some structural changes in the polymer matrix probably occurred.

For extensive stages of swelling, the following equation should be used:[55]

$$\frac{t}{SD} = A + Bt \quad (9)$$

where $B = 1/SD_{eq}$ is the reciprocal of the equilibrium swelling degree and $A = 1/v_0$ is the reciprocal of the initial swelling rate. Equation (9) represents the Schott second-order kinetics.

To model the kinetics of swelling, the first-order equation is used:

$$\frac{SD}{SD_{eq}} = 1 - \exp(-Kt) \quad (10)$$

The obtained results [from eq. (9)] showed that the values of the initial swelling rate for all of the investigated nano-Ag/PVA

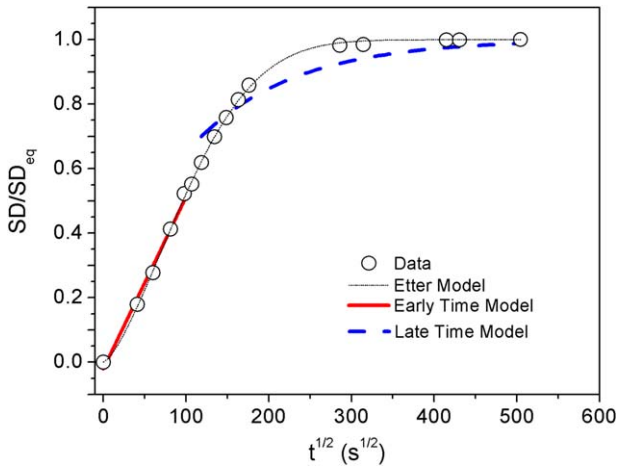

Figure 5. Representative model fits for early time, late time, and Etters approximations of diffusion through the samples (sample S3 in an SBF solution at 37°C); $t^{1/2}$ is the square root of time. [Color figure can be viewed in the online issue, which is available at wileyonlinelibrary.com.]

hydrogel systems were greater compared to that of the pure PVA hydrogel.

The diffusion coefficients (D) for both the PVA hydrogel and nano-Ag/PVA hydrogel device were determined by the models based on solutions of Fick's law with three approximations: the early time approximation [eq. (11), valid for the first 60% of sorption], late time approximation [eq. (12), valid for the latter 40% of sorption], and Etters approximation [eq. (13)]:[53]

$$\frac{SD}{SD_{eq}} = 4\left[\frac{Dt}{\pi\delta^2}\right]^{\frac{1}{2}} \tag{11}$$

$$\frac{SD}{SD_{eq}} = 1 - \frac{8}{\pi^2}\exp\left(-\frac{D\pi^2 t}{\delta^2}\right) \tag{12}$$

$$\frac{SD}{SD_{eq}} = 1 - \exp\left[-k\left(\frac{Dt}{\delta^2}\right)^a\right]^{\frac{1}{b}} \tag{13}$$

An example of the model fits is shown in Figure 5 and is representative of the data reported in this article.

The results are listed in Table III. The obtained values of the early time and the late time diffusion coefficient [D (cm^2/s)] for samples S1, S2, and S3 were slightly different compared to the values for the PVA hydrogel. Also, no significant difference between the diffusion coefficients of the early and the late time were observed for given experimental conditions. For the higher C of Ag nanoparticles in samples S4, S5, and S6, the diffusion coefficients of the early and the late time approximations were greater compared to that of the PVA hydrogel (sample S7). The highest value was obtained for sample S4.

The values of the diffusion coefficient calculated by the Etters model for samples S2, S3, and S4 were greater compared to that of the pure PVA hydrogel. For samples S1, S5, and S6, the values were lower than that for the pure PVA hydrogel.

Quantification of the *In Vitro* Release of the Ag^+ Ions

A sustained, steady supply of active Ag is an important property in antimicrobial material. The release of Ag^+ ions from the nano-Ag/PVA hydrogel device was continuous during a long period of time; this indicated that, in general, the investigated hydrogel nanosystems met that criteria.

In general, Ag can be released both in the ionic and particulate forms; therefore, a reliable kinetic sample during the test might affect the release kinetics, but that effect was not in the scope of this study. In the case of the investigated nano-Ag/PVA hydrogel device, the main released form of Ag was ionic because Ag nanoparticles were encapsulated in the matrix, and this prevented their release into the environment in larger amounts.

It was observed recently that Ag nanoparticles are unstable under physiological conditions to some extent because of their large ionic strength, which modifies the particle formal charge.[56] However, in general, studies have shown that the most of the Ag^+ ions are formed by oxidation of the zero-valent metallic particles, typically by reaction with dissolved O_2 and mediated by protons and other components in the surrounding fluid phase.[41] The nanoparticles undergo the following redox reaction and the release of Ag^+ ions:[57]

$$2Ag_{(s)} + \frac{1}{2}O_{2(aq)} + 2H^+ \rightarrow 2Ag^+_{(aq)} + H_2O_{(aq)} \tag{14}$$

Because the release of soluble silver from Ag surfaces is primarily a heterogeneous oxidation reaction involving the cooperative effects of dissolved oxygen and protons, this suggests SA dependence and the potential to control the release through particle size control.[57]

The obtained *in vitro* release profiles are shown in Table IV, where the silver ions that were released to medium are expressed as cumulative Ag^+ ion concentration released versus time per mass of hydrogel.

The obtained patterns were similar to those observed for the other drugs. For a smaller initial C of Ag nanoparticles (sample S2), the release profile showed the initial rapid release of silver in comparison to the release from sample S3, even though it contained less Ag. The higher initial release, as shown in Figure 5, in a duration of 3 days from sample S2 could be associated with the smaller particle size, greatest SA of the Ag nanoparticles, and consequently, their greater solubility, as shown in Table I. For a higher C of Ag nanoparticles (S4, S5, and S6), an initial rapid release of Ag^+ ions was observed for all of the samples. This initial burst of Ag^+ ions was found to be critical in relation to the antibacterial properties of the materials. The achievement of immediate antibacterial concentrations in contact with body fluids followed by a lower and maintained release was sufficient to preserve the antibacterial concentrations of Ag^+ ions over a period of time and to reduce the initial bacterial attachement.[58]

Because the experiments were performed at physiological pH and were buffered, the overall cell voltage and the Gibbs free energy for eq. (14) were calculated according to the Nernst expression [14a and 14b, respectively] to obtain the bactericidal effectiveness and system thermodynamics that provided the killing power of the nano-Ag/PVA device:

Table III. Summary of the Media Diffusion Coefficients (*D*s)

	Early time approximation		Late time approximation		Etters model approximation	
Sample	$D \times 10^7$ (cm^2/s)	R^2	$D \times 10^7$ (cm^2/s)	R^2	$D \times 10^8$ (cm^2/s)	R^2
S1	1.40	0.98	1.32	0.99	4.66	0.99
S2	1.16	0.99	1.19	0.99	7.32	0.99
S3	1.25	0.99	1.25	0.99	5.46	0.99
S4	8.51	0.98	8.14	0.98	53.3	0.99
S5	4.26	0.99	4.49	0.98	4.78	0.99
S6	4.81	0.98	5.17	0.85	0.12	0.98
S7	1.49	0.99	1.41	0.99	5.24	0.99

$$E_{\text{cell}} = \left(E^o_{O_2/O^{2-}} - E^o_{\text{NP}}\right) - \frac{RT}{nF} \ln \frac{[Ag^+]^2[H_2O]}{[Ag]^2[O_2]^{\frac{1}{2}}[H^+]^2} \quad (14a)$$

$$\Delta G = -nFE_{\text{cell}} \quad (14b)$$

where E_{cell} is the overall cell voltage, $E^o_{O_2/O^{2-}} = E^o_c = 1.23$ V, E°c is the cathode standard electrode potential, $E^o_{Ag/Ag^+} = E^o_a = -0.799V$, E°_a is the anode standard electrode potential, $E^o_{AgNPs/Ag^+} = E^o_{Ag/Ag^+} - E^o_{Plieth}$, (AgNPs are silver nanoparticles) $E^o_{cell} = E^o_{O_2/O^{2-}} - E^o_{AgNPs/Ag^+}$, where E°_{cell} is the standard cell electrode potential, n is the number of electrons transferred, and F is Faraday's constant. The variation in the formal potential of oxidation is expressed as $E^o_{Plieth} = 2\gamma v_M/zFr$, where v_M is the molar volume of the bulk Ag and z is the lowest valence state. Namely, Plieth[59] predicted a negative shift in the Ag standard electrode potential and a decrease in the work function of the small metallic particles (<25 nm). This means that smaller metal nanoparticles are more easily oxidized than bulk materials. The difference in standard electrode potentials causes differences in the equilibrium silver ion concentration around each particle.[59]

The parameters of oxygen solubility in eq. (14a) were obtained from Henry's law at the stated experimental conditions: $[H_2O]/([O_2]^{1/2}[H^+]^2) = k_{HL} = 3.181 \times 10^{-2}$, where k_{HL} is the Henry's law constant. The concentrations of the Ag^+ ions ($[Ag^+]$) in eq. (14a) were taken as the cumulative released concentrations, whereas the concentrations of nano-Ag ([Ag]) were taken as the cumulatively reduced initial concentration.

Figure 6(a–c) shows the cell potential, a plot of the shift in the standard electrode potential of the silver particles and the corresponding standard cell electrode potential as a function of r and Gibbs free energy. The cell voltage mainly increased with the initial concentration of silver. The highest value obtained for sample S4 was probably the result of the greatest fluid diffusion coefficient (D), as shown in Table III. It seemed that the cell potential depended on the fluid diffusion characteristics. We assumed that when the initial concentration of silver was 1 (for bulk silver), the cell potential of the investigated nanosystems would have the highest value for the sample with the smallest nanoparticles [S2; Figure 6(a), inset]. The obtained results for the Gibbs free energy, calculated from eq. [14b] and depicted in Figure 6(c), show that the driving force for the oxidation increased with the initial concentration of silver and the fluid diffusion characteristics under physiological conditions. The largest was for sample S4. In addition, the altered nanoscale thermodynamics of the metallic particles, because of the increased surface energy, contributed to the calculated total values of the Gibbs free energy.[60]

Throughout the duration of the experiment, that is, after 9 days, there was a difference in the final cumulative silver released throughout the study. The percentage of released Ag^+ ions declined along with the increasing total concentration of Ag^+ ions doped in the device, as shown in Table IV. The release of Ag^+ ions from the nano-Ag/PVA hydrogel device for higher *C*s of Ag nanoparticles were inhibited by oxygen depletion or by high concentrations of free Ag^+ ions, which could interact with the surfaces of the nanoparticles and inhibit surface reactions.[61]

Silver shows bactericidal activity at concentrations as low as 0.035 ppm without toxic effects to mammalian cells.[62] However, the typical minimum inhibitory concentration (MIC) and minimum bactericidal concentration (MBC) against standard reference cultures and multi-drug-resistant organisms are 0.78–6.25 and 12.5 ppm, respectively.[6] A silver concentration of up to 1.2 ppm has no cytotoxic effect on fibroblasts *in vitro*, which play a critical role in wound healing. However, in general, cytotoxic effects seem to be dose-depenent.[63] The maximum toxic concentration for human cells is around 10 ppm.[64] However, some authors have suggested that for topical use, Ag nanoparticles induce apoptosis at concentrations of up to 250 μg/mL (ppm), which could favor scarless wound healing.[6]

Table IV. Cumulative *In Vitro* Ag^+ Ion Release from the Nano-Ag/PVA Hydrogel Device per Mass of the hydrogel nanocomposite (HG NC)

	Cumulative silver release/mass of HG NC (ppm/g)					
t (days)	S1	S2	S3	S4	S5	S6
1	5.8	6.6	5.4	29.8	95.0	212.1
3	9.5	10.0	11.1	47.6	183.7	336.9
5	12.4	12.5	15.1	59.1	193.6	356.3
7	15.5	15.4	18.7	70.6	199.6	364.8
9	18.9	18.5	22.3	80.4	206.1	377.9
%/g of HG NC	16	19	11	4	4	7

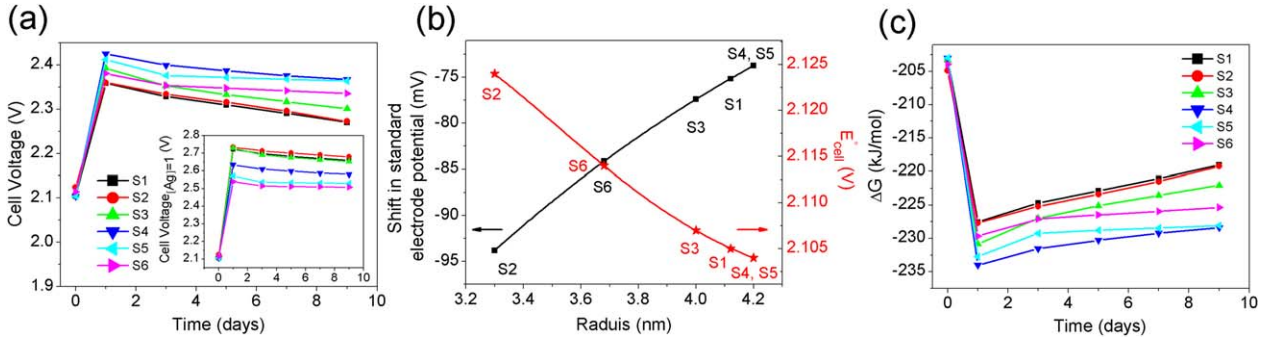

Figure 6. (a) Cell potential, (b) plot of the shift in the standard electrode potential of the Ag nanoparticles and corresponding standard cell electrode potentials (E°_{cell}) as a function of radius (r), and (c) Gibbs free energy (ΔG) (all values are expressed per gram of HG NC). [Color figure can be viewed in the online issue, which is available at wileyonlinelibrary.com.]

Except for their use as a antimicrobial topical dressings, nano-Ag/hydrogel systems could be applied for orthopedic implants, such as artificial cartilage, intervertebral discs, and artificial menisci[65] or tissue expander devices. Many biomaterials are being developed for use in cartilage, including meniscus substitution and hemiarthroplasty implants, but crosslinked PVA hydrogels, because of their good biocompatibility and extraordinary properties, such as low elastic modulus and high resilient and a similar biphasic lubrication mechanism is promising kind.[66–68]

Kinetic Aspects and Diffusion Model of the *In Vitro* Release of the Ag^+ Ions from Nano-Ag/PVA Hydrogel Device. The curvilinear nature of the cumulative percentage of released silver versus time plots suggests that silver release from the hydrogel does not follow zero-order kinetics. The models used to fit obtained Ag^+ ion release data were as follows:[69,70]

1. Korsmeyer–Peppas model:

$$\frac{M_t}{M_\infty} = k_{KP}\, t^n \tag{15}$$

This describes the drug release from a polymeric system by a simple relationship, where M_t is the amount of drug released at time t; M_∞ is the mass of drug doped into the device at equilibrium; k_{KP} is the Korsmeyer–Peppas constant, which incorporates the characteristics of the macromolecular network or particle system that makes up the formulation; and n is the release exponent that describes the drug-release (transport) mechanism.

2. Higuchi model, which describes the release of drugs from an insoluble matrix as a square root of a time-dependent process based on Fickian diffusion:

$$\frac{M_t}{M_\infty} = k_H\, t^{1/2} \tag{16}$$

3. The Hixson–Crowell cube root law, which defines the release from systems by dissolution where there is a change in the SA and the diameter of the particles:

$$(M_t - M_\infty)^{1/3} = k_{HC}\, t \tag{17}$$

where k_{HC} is the Hixson–Crowell constant.

4. The Kopcha model, which describes how to quantify the contributions of diffusion and polymer relaxation:

$$\frac{M_t}{M_\infty} = At^{1/2} + Bt \tag{18}$$

where A and B are the Kopcha constants.

5. Makoid–Banakar's pharmacokinetic dissolution model:

$$\frac{M_t}{M_\infty} = k_{MB}\, t^n e^{-ct} \tag{19}$$

where k_{MB} is Makoid–Banakar's constant.

Modeling was performed with the parameters of a nonlinear function that provided the closest fit between the experimental observations and the nonlinear function (Figure 7). The data modeling results are summarized in Table V. The results of the curve-fitting studies revealed that Ag^+ ions released from the nano-Ag/PVA hydrogel device could be described by all of the previous models. The models that gave the best fit solution ($R^2 = 0.99$) were the Kopcha and Makoid–Banakar models (Figure 7 and Table V). The Hixson–Crowell model also had good correlation coefficients. Good fitting release data of the Hixson–Crowell model suggests that the Ag nanoparticles' SA changed as a function of time.

Classification of the diffusion of fluid in hydrogels in general can also be used to classify drug-release profiles from polymers.[54,73] The Korsmeyer–Peppas release exponent was less than 0.5 for S2, S4, S5, and S6; this suggested that the diffusion rate was controlled by the mass transport rate because of a concentration gradient of Ag^+ ions (Fickian diffusion).[74] This finding should have been supported by the evaluation of the ratios of the terms A/B derived from the Kopcha model because the Kopcha model could also be used to quantify the relative contributions of the diffusion and polymer relaxation to Ag^+ ion release (i.e., underlying mass transport mechanism). The data in Table V clearly show that the value of A was far greater than that for B for all of the investigated nanosystems; this suggested that Ag^+ ion release was predominantly controlled by a diffusion process. Moreover, as shown in Table V, Makoid–Banakar's parameter (n_{MB}; related to the shape of the function) was smaller for sample S2. When n_{MB} was smaller, the faster Makoid–Banakar's function ramped up; that is, the release of

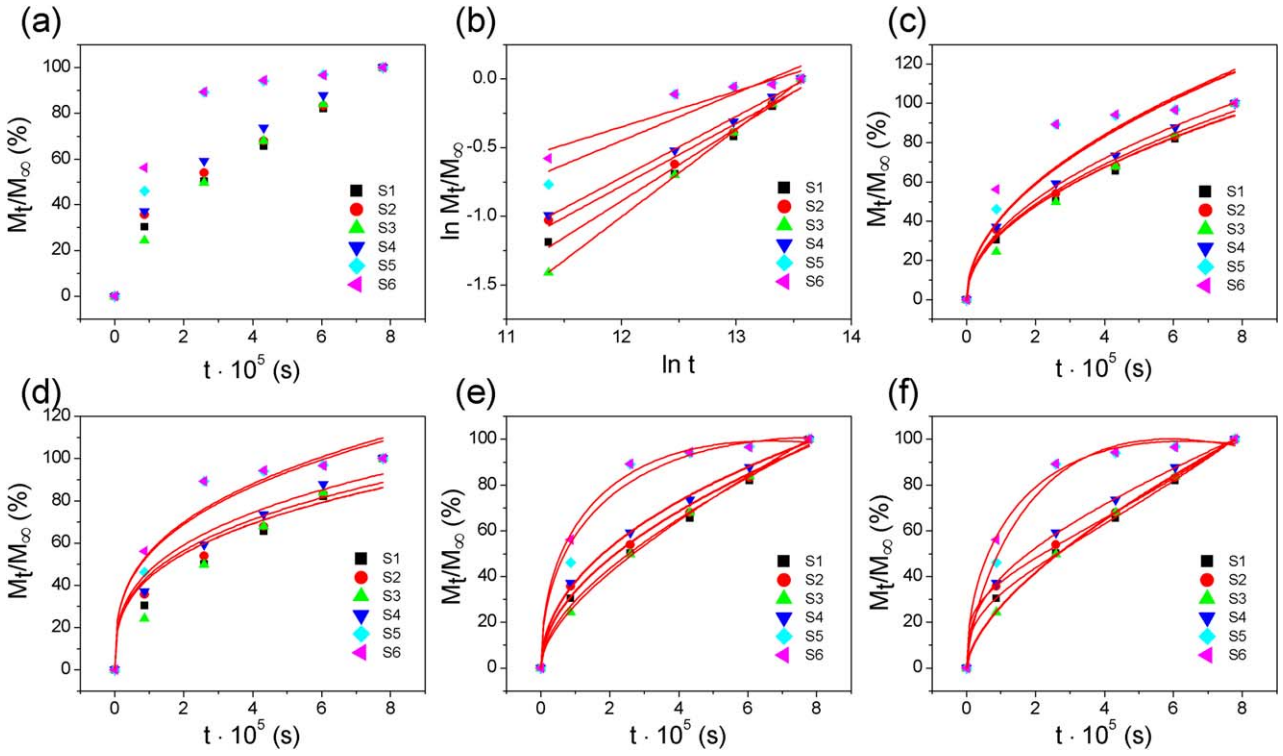

Figure 7. Mathematical modeling of Ag^+ ion release from the nano-Ag/PVA hydrogel device: (a) cumulative released amount of Ag^+ ions (%), (b) Korsmeyer–Peppas model, (c) Higuchi model, (d) Hixson–Crowel model, (e) Kopcha model, and (f) Makoid–Banakar model. [Color figure can be viewed in the online issue, which is available at wileyonlinelibrary.com.]

Ag^+ ions was rapid. The previous analysis indicated that the kinetics of Ag^+ ion release were related to the size of the nanoparticles; namely, the smaller particles showed faster Ag^+ ion release. This was in accordance with the previous assumption that the release of Ag^+ ions would depend on the SA of the nanoparticles.[64]

In addition, the short time approximated Ag^+-ion diffusion constant (D_{Ag}) was calculated from the following equation, which was derived from Fick's second law of diffusion for the drug release in the case of slablike devices:[71,72]

$$\frac{M_t}{M_0} = 4\left(\frac{Dt}{\pi\delta^2}\right)t^{1/2} \tag{20}$$

where M_0 is the total mass of drug doped into the device, D is the diffusion coefficient of the drug within the polymer matrix, and δ is the thickness of the device. This is an early time approximation that holds for the first 60% of cumulative release, that is, $0 \leq M_t/M_0 \leq 0.6$.

The calculated values from eq. (20) and Figure 8 are shown in Table VI. D_{Ag} was found to be slightly greater for S2, that is, for the hydrogel nanosystem containing the smallest Ag nanoparticles.

Finally, the kinetic models could be used to predict the performance and the possible lifetime of the nano-Ag/PVA hydrogel device applied in different environments.

In clinical practice, antimicrobial wound dressings are changed after 48 or 72 h. It has been recommended that silver-containing antimicrobial dressings should be used for 2 weeks initially, and then, the wound, the patient, and the management should be re-evaluated.[66] Therefore, in the case of the investigated nano-Ag/PVA hydrogel device, the amounts of Ag^+ ions delivered after 48 or 72 h would be (in ppm/g of HG NC, as calculated with Makoid–Banakar's pharmacokinetic model): 7.7 (S1), 8.4 (S2), 8.5 (S3), 39.7 (S4), 144.6 (S5), and 284.0 (S6) after 48 h and 9.5 (S1), 10.0 (S2), 10.9 (S3), 47.5 (S4), 172.6 (S5), and 324.3 (S6) after 72 h. The released Ag^+ ion concentration after 48 h from samples S1, S2, and S3 were in the range of MIC, whereas from the samples S4, S5, and S6, they were in the range of MBC. On the other hand, after 72 h, all of the investigated samples released Ag^+ ions in the MBC range. The final concentrations of released Ag^+ ions to the wound site after 15 days (ppm/g of HG NC) would be 57.7 (S1), 63.0 (S2), 63.7 (S3), 297.7 (S4), 1084.5 (S5), and 2130.0 (S6) when the dressings were changed after 48 h and 47.0 (S1), 49.5 (S2), 54.5 (S3), 236.5 (S4), 862.5 (S5), and 1621.0 (S6) when the dressings were changed after 72 h. Because, in a wound environment, the Ag^+ ions interact with wound components such as chloride ions and proteins or wound debris, the only a small proportion of silver presented to a wound site in a dressing is systemically absorbed. Therefore, silver dressings are unlikely to cause true argyria.[66] According to the obtained released data, the investigated nano-Ag/hydrogel device and samples S1, S2, and S3 could be safely used as an antimicrobial topical dressing for a duration of 15 days. Even with higher molar concentrations of Ag nanoparticles, sample S4 could be used safely when scarless wound healing is needed.

Finally, the Makoid–Banakar's model was used to predict performance and the possible lifetime of the nano-Ag/PVA

Table V. Results of the Model Fitting of the Ag^+ Ion Release Profiles

	Korsmeyer–Peppas			Higuchi		Hixson–Crowel	
Sample	k_{KP} (%/s^n)	N	R^2	k_H (%/s$^{1/2}$)	R^2	k_{HC} (%/s$^{1/3}$)	R^2
S1	0.071	0.53	0.98	0.106	0.99	0.942	0.93
S2	0.189	0.46	0.98	0.109	0.99	0.969	0.96
S3	0.018	0.64	0.99	0.107	0.98	0.943	0.91
S4	0.231	0.45	0.99	0.114	0.99	1.014	0.98
S5	0.975	0.35	0.83	0.132	0.89	1.183	0.96
S6	3.099	0.26	0.86	0.133	0.85	1.199	0.96
	Kopcha			Makoid–Banakar			
	A (%/s$^{1/2}$)	$B \times 10^5$ (%/s)	R^2	k_{MB} (%/s)	n	$c \times 10^7$	R^2
S1	0.083	3.09	0.99	0.597	0.34	−6.22	0.99
S2	0.104	0.68	0.99	1.899	0.25	−6.71	0.99
S3	0.072	4.63	0.99	0.022	0.62	−0.55	0.99
S4	0.123	−1.24	0.99	0.483	0.38	−2.20	0.99
S5	0.222	−12.2	0.98	0.023	0.68	11.50	0.99
S6	0.243	−14.8	0.99	0.245	0.49	7.71	0.99

c is the parameter of the model subjected to the constraint that the total dissolution of the drug dose must occur at the same time as the maximum value of the Makoid-Banakar function.

hydrogel device if it is applied as a soft tissue implant (meniscus) in a synovial joint (e.g., the knee). Namely, the volumes of the lateral and medial meniscus are 1.8–2.4 cm^3, and they consist of water (60–70%), collagen (15–20%), and proteoglycans (1–2%).[74] The intra-articular synovial fluid (SF) volume for lavaged knees ranges from 0.555 to 71.71 mL, with a median volume of 3.048 mL.[75] It undergoes continuous turnover by trans-synovial flow into synovial lymph vessels within a period of 2 h or less.[65] Therefore, the concentrations of Ag^+ ions in the intra-articular SF (in ppm), released from the same nano-Ag/PVA hydrogel device, if potentially implanted in the knee as both lateral and medial menisci, after the 2 h needed for the complete replacement of SF (for a median volume of SF of 3.048 mL), would be approximately 3.4 (S1), 4.6 (S2), 1.9 (S3), 16.8 (S4), 33.0 (S5), and 107.0 (S6). As silver has bactericidal activity at a concentration as low as 0.035 ppm,[64] the concentrations of Ag^+ ions released from samples S1, S2, and S3 would be sufficient to preserve the postoperation sterility of implanted devices. In addition, they were below the maximum toxic concentration for human cells (ca. 10 ppm).[58]

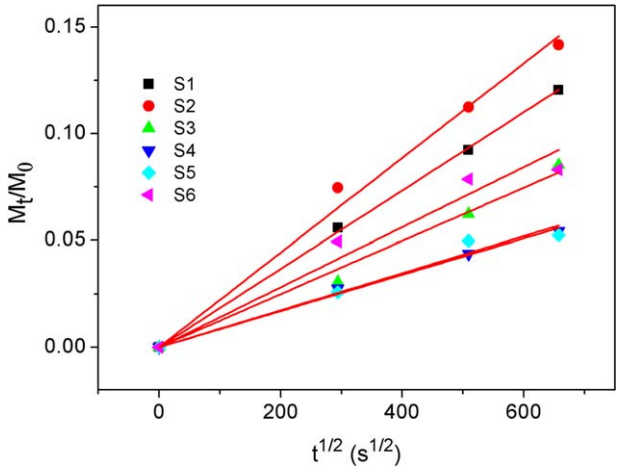

Figure 8. Model fits for the early time approximation of the Fickian diffusion of Ag^+ ions from the nano-Ag/PVA hydrogel device. [Color figure can be viewed in the online issue, which is available at wileyonlinelibrary.com.]

Antibacterial Potential. To investigate the possibility of predicting the antibacterial potential with a cumulative silver release study, samples with an average weight of 0.113 g were investigated. The calculated concentrations of Ag^+ ions released to the medium (in parts per million) from nano-Ag/PVA hydrogel samples of that size after 24 h during the *in vitro* agar plate test were 0.66 (S1), 0.74 (S2), 0.61(S3), 3.37(S4), 10.74 (S5), and 23.96 (S6). The values obtained for samples S1, S2, and S3 were at the lower limit of the MIC concentration range (estimated to be 0.78–6.25 ppm[6]), although it was suggested that concentrations as low as 0.035 ppm[64] had bactericidal activity. On the other hand, this calculation predicted that concentrations of Ag^+ ions released from samples S4, S5, and S6 had good antibacterial potential.

Figure 9(a,b) illustrates the results obtained for samples S1, S2, S3, and S7 (pure PVA). The concentration level capable of rendering antimicrobial potential and the conditions for achieving significant antimicrobial activity were not met in the duration of the experiment for samples S1, S2, and S3. Figure 9(c,d) illustrates the obtained antibacterial potential for samples S4, S5, and S6 against Gram-positive *S. aureus* and Gram-negative *E. coli* cultures upon immersion in buffered solution for 2 weeks and 2 months. After 24 h of incubation, despite smaller or larger losses of silver, these nano-Ag/PVA hydrogel devices retained excellent antibacterial activity against both *S. aureus* and *E. coli*. The formation of inhibition zones was clearly seen,

Table VI. Summary of the Ag^+ Ion Diffusion Coefficients

Sample	$D \times 10^{10}$ (cm^2/s)	R^2
S1	1.48	0.99
S2	2.17	0.99
S3	0.68	0.99
S4	0.32	0.99
S5	0.23	0.99
S6	0.56	0.98

with slightly larger diameters in the case of *S. aureus*. As a control, the pure PVA hydrogel showed no significant inhibition ability [Figure 9(a,b)], although it was reported that PVA itself had strong antimicrobial properties.[76] In addition, longitudinally severed samples of the gels were tested [indicated by arrows in Figure 9(c,d)]. The inhibition zone existed, although it was smaller, and this confirmed the predicted effect of sample mass reduction on the antibacterial potential.

CONCLUSIONS

In this study, a nano-Ag/PVA hydrogel device was synthesized by *in situ* γ irradiation with the aim of designing a hydrogel controlled release system of Ag^+ ions for antibacterial purposes with the advantages of the radiolytic method. The *in vitro* Ag^+ ion release study showed sustained and controlled release in a solution with a pH similar to that of biological fluids, with the absolute amount of the Ag^+ ions released in the antimicrobial parts per million concentration range. The obtained *in vitro* release profiles of silver were similar to the patterns observed with other drugs. Therefore, the elements of the drug-delivery paradigm were applied for the study of Ag^+ ion release kinetics. The models that gave the best fit solution between the experimental observations and the nonlinear function were the Kopcha and Makoid–Banakar's pharmacokinetic dissolution models. From the ratios of the term *A*/*B*, derived from the Kopcha model, we found that the release of Ag^+ ions was predominantly controlled by a diffusion process, that is, the mass transport rate due to a concentration gradient of Ag^+ ions (Fickian diffusion). The Ag^+ ion release

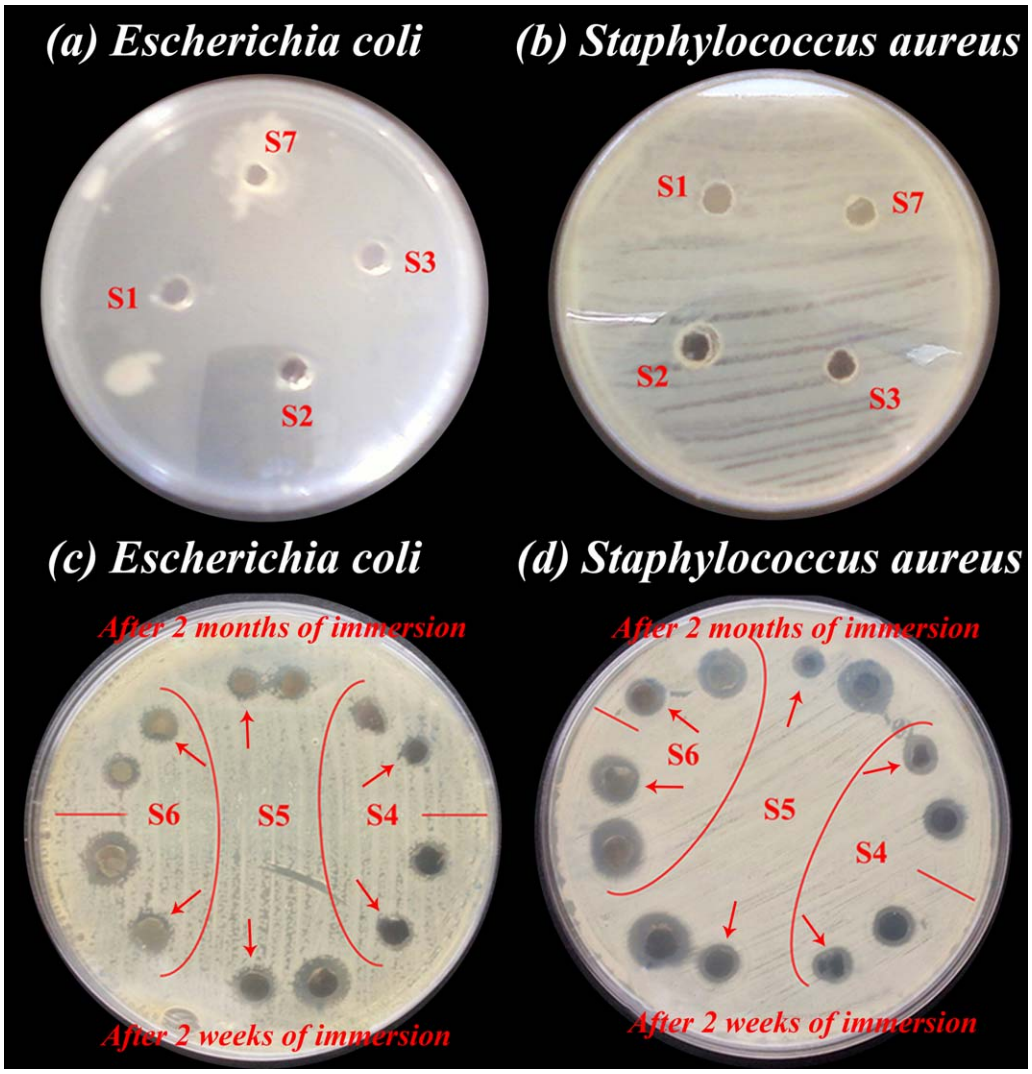

Figure 9. Test of the antimicrobial activity against (a,c) *E. coli* and (b,d) *S. aureus*. Longitudinally severed samples of the gels are indicated by arrows. [Color figure can be viewed in the online issue, which is available at wileyonlinelibrary.com.]

characteristics were the result not only of the *C* but also the size of Ag nanoparticles. This outcome was in agreement with the greater theoretical SA and solubility of the smaller Ag nanoparticles (calculated by Ostwald–Freundlich equation, whose dimensions were determined by means of a UV–vis sizing technique and XRD structural analysis). However, it appeared that the cell oxidation potential of Ag nanoparticles depended on the diffusion characteristics of the fluids penetrating into the Ag/PVA nanosystem.

Finally, antimicrobial testing showed a correlation between the observed Ag^+ ion release potential and the antimicrobial properties of the nano-Ag/PVA hydrogel device against Gram-positive *S. aureus* and Gram-negative *E. coli*.

According to the obtained results, we expect that the used mathematical models could be routinely applied to help optimize the novel nano-Ag/hydrogels dosage forms. This is not only of academic interest, but it is a prerequisite for the efficient improvement of the safety of silver pharmacotreatments.

ACKNOWLEDGMENTS

This work was financed by the Ministry of Education, Science, and Technological Development of the Republic of Serbia (project III 45005) and by the International Atomic Energy Agency (project CRP:F22051, contract 16733).

REFERENCES

1. Hoffman, A. S. *Adv. Drug Delivery Rev.* **2002**, *54*, 3.
2. Hilton, J. R.; Williams, D. T.; Beuker, B.; Miller, D. R.; Harding, K. G. *Clin. Infect. Dis.* **2004**, *39*, 100.
3. Kim, J. S.; Kuk, E.; Yu, K. N.; Kim, J. H.; Park, S. J.; Lee, H. J.; Kim, S. H.; Park, Y. K.; Park, Y. H.; Hwang, C. Y.; Kim, Y. K.; Lee, Y. S.; Jeong, D. H.; Cho, M. H. *Nanomed.-Nanotechnol.* **2007**, *3*, 95.
4. Qureshi, A. T.; Landry, J. P.; Dasa, V.; Janes, M.; Hayes, D. J. *J. Biomater. Appl.* **2013**, *0*, 1.
5. Inbaneson, S. J.; Ravikumar, S.; Manikandan, N. *Appl. Nanosci.* **2011**, *1*, 231.
6. Jain, J.; Arora, S.; Rajwade, J. M.; Omray, P.; Khandelwal, S.; Paknikar, K. M. *Mol. Pharm.* **2009**, *6*, 1388.
7. Madhumathi, K.; Kumar, P. T. S.; Abhilash, S.; Sreeja, V.; Tamura, H.; Manzoor, K.; Nair, S. V.; Jayakumar, R. *J. Mater. Sci.: Mater. Med.* **2010**, *21*, 807.
8. Zan, X.; Kozlov, M.; McCarthy, T. J.; Su, Z. *Biomacromolecules* **2010**, *11*, 1082.
9. Davis, S. C.; Martinez, L.; Kirsner, R. *Curr. Diabetes Rep.* **2006**, *6*, 439.
10. Xiu, Z.; Zhang, Q.; Puppala, H. L.; Colvin, V. L.; Alvarez, P. J. *J. Nano Lett.* **2012**, *12*, 4271.
11. Liu, J.; Sonshine, D. A.; Shervani, S.; Hurt, R. H. *ACS Nano* **2010**, *4*, 6903.
12. Gupta, A.; Kumar, R.; Upadhyay, N. K.; Surekha, P.; Roy, P. K. *J. Appl. Polym. Sci.* **2009**, *111*, 1400.
13. Abd El-Mohdy, H. L.; Safrany, A. *Radiat. Phys. Chem.* **2008**, *77*, 273.
14. Singh, R.; Singh, D. *J. Mater. Sci:. Mater. Med.* **2012**, *23*, 2649.
15. Kačarević-Popović, Z.; Tomić, S.; Krklješ, A.; Mićić, M.; Suljovrujić, E. *Radiat. Phys. Chem.* **2007**, *76*, 1333.
16. Jovanović, Ž.; Krklješ, A.; Stojkovska, J.; Tomić, S.; Obradović, B.; Mišković-Stanković, V.; Kačarević-Popović, Z. *Radiat. Phys. Chem.* **2011**, *80*, 1208.
17. Krklješ, A.; Nedeljković, J.; Kačarević-Popović, Z. *Polym. Bull.* **2007**, *58*, 271.
18. Kačarević-Popović, Z.; Dragašević, M.; Krklješ, A.; Popović, S.; Jovanović, Ž.; Tomić, S.; Mišković-Stanković, V. *Open Conf. Proc. J.* **2010**, *1*, 200.
19. Choi, S. H.; Zhang, Y. P.; Gopalan, A.; Lee, K. P.; Kang, H. D. *Colloids Surf. A* **2005**, *256*, 165.
20. Rao, Y. N.; Banerjee, D.; Datta, A.; Das, S. K.; Guin, R.; Saha, A. *Radiat. Phys. Chem.* **2010**, *79*, 1240.
21. Naghavi, K.; Saion, E.; Rezaee, K.; Yunus, W. M. M. *Radiat. Phys. Chem.* **2010**, *79*, 1203.
22. Rattanaruengsrikul, V.; Pimpha, N.; Supaphol, P. *J. Appl. Polym. Sci.* **2012**, *124*, 1668.
23. Varaprasad, K.; Mohan, Y. M.; Ravindra, S.; Reddy, N. N.; Vimala, K.; Monika, K.; Sreedhar, B.; Raju, K. M. *J. Appl. Polym. Sci.* **2010**, *115*, 1199.
24. Lee, W. F.; Tsao, K. T. *J. Appl. Polym. Sci.* **2006**, *100*, 3653.
25. Valle, H.; Rivas, B. L.; Aguilar, M. R.; Román, J. S. *J. Appl. Polym. Sci.* **2013**, *129*, 537.
26. Lee, W. F.; Huang, Y. C. *J. Appl. Polym. Sci.* **2007**, *106*, 1992.
27. Ahmed, E. M.; Aggor, F. S. *J. Appl. Polym. Sci.* **2010**, *117*, 2168.
28. Varaprasad, K.; Mohan, Y. M.; Vimala, K.; Raju, K. M. *J. Appl. Polym. Sci.* **2011**, *121*, 784.
29. Li, G.; Wen, Q.; Zhang, T.; Ju, Y. *J. Appl. Polym. Sci.* **2013**, *127*, 2690.
30. Chang, H. W.; Lin, Y. S.; Tsai, Y. D.; Tsai, M. L. *J. Appl. Polym. Sci.* **2013**, *127*, 169.
31. Singh, B. *Int. J. Pharm.* **2007**, *334*, 1.
32. Kokubo, T.; Kushitani, H.; Sakka, S.; Kitsugi, T.; Yamamuro, T. *J. Biomed. Mater. Res.* **1990**, *24*, 721.
33. Peña, O.; Rodríguez-Fernández, L.; Roiz, J.; Cheang-Wong, J. C.; Arenas-Alatorre, J.; Crespo-Sosa, A.; Oliver, A. *Rev. Mex. Fis.* **2007**, *53*, 62.
34. Dakhel, A. A.; Henari, F. Z. *Int. J. Nanosci.* **2011**, *10*, 433.
35. Tadd, E.; Zeno, A.; Zubris, M.; Dan, N.; Tannenbaum, R. *Macromolecules* **2003**, *36*, 6497.
36. Rance, G. A.; Marsh, D. H.; Khlobystov, A. N. *Chem. Phys. Lett.* **2008**, *460*, 230.
37. Veenas, C. L.; Nissamudeen, K. M.; Smitha, S. L.; Biju, V.; Gopchandran, K. G. *J. Optoelectron. Adv. Mater.* **2009**, *11*, 114.
38. Stepanov, A. L.; Hole, D. E.; Townsend, P. D. *Nucl. Instrum. Methods B* **1999**, *149*, 89.
39. Liu, X.; Atwater, M.; Wang, J.; Huo, Q. *Colloids Surf. B* **2007**, *58*, 3.

40. Wani, I. A.; Ganguly, A.; Ahmed, J.; Ahmad, T. *Mater. Lett.* **2011**, *65*, 520.
41. Ma, R.; Levard, C.; Marinakos, S. M.; Cheng, Y.; Liu, J.; Michel, F. M.; Brown, G. E.; Lowry, G. V. *Environ. Sci. Technol.* **2012**, *46*, 752.
42. Liu, J.; Sonshine, D. A.; Shervani, S.; Hurt, R. H. *ACS Nano* **2010**, *4*, 6903.
43. George, J.; Sajeevkumar, V. A.; Ramana, K. V.; Sabapathy, S. N.; Siddaramaiah, B. S. M. *J. Mater. Chem.* **2012**, *22*, 22433.
44. Radosavljević, A.; Bozanić, D.; Bibić, N.; Mitrić, M.; Kačarević-Popović, Z.; Nedeljković, J. *J. Appl. Polym. Sci.* **2012**, *125*, 1244.
45. Peppas, N. A. *Pharm. Acta Helv.* **1985**, *60*, 110.
46. Tomić, S.; Mićić, M.; Filipović, J.; Suljovrujić, E. *Radiat. Phys. Chem.* **2007**, *76*, 801.
47. Can, H. K.; Denizli, B. K.; Kavlak, S.; Guner, A. *Radiat. Phys. Chem.* **2005**, *72*, 483.
48. Kaplan, H.; Guner, A. *J. Appl. Polym. Sci.* **2000**, *78*, 994.
49. Dole, M.; Faller, I. L. *J. Am. Chem. Soc.* **1950**, *72*, 414.
50. Li, H.; Hardy, R. J.; Gu, X. *AAPS PharmSciTech* **2008**, *9*, 437.
51. Luo, Y. L.; Wei, Q. B.; Xu, F.; Chen, Y. S.; Fan, L. H.; Zhang, C. H. *Mater. Chem. Phys.* **2009**, *118*, 329.
52. Jovanović, J.; Adnađević, B. *Polym. Bull.* **2007**, *58*, 243.
53. Mullarney, M. P.; Seery, T. A. P.; Weiss, R. A. *Polymer* **2006**, *47*, 3845.
54. Ritger, P. L.; Peppas, N. A. *J. Controlled Release* **1987**, *5*, 37.
55. Katime, I.; Velada, J. L.; Novoa, R.; Díaz de Apodaca, E. *Polym. Int.* **1996**, *40*, 281.
56. Alarcon, E. I.; Bueno-Alejo, C. J.; Noel, C. W.; Stamplecoskie, K. G.; Pacioni, N. L.; Poblete, H.; Scaiano, J. C. *J. Nanopart. Res.* **2013**, *15*, 1374.
57. Lee, Y. J.; Kim, J.; Oh, J.; Bae, S.; Lee, S.; Hong, I. S.; Kim, S. H. *Environ. Toxicol. Chem.* **2012**, *31*, 155.
58. Jamuna-Thevi, K.; Bakar, S. A.; Ibrahim, S.; Shahab, N.; Toff, M. R. M. *Vacuum* **2011**, *86*, 235.
59. Redmond, P.; Hallock, A.; Brus, L. *Nano Lett.* **2005**, *5*, 131.
60. Brainina, K. Z.; Galperin, L. G.; Kiryuhina, T. Y.; Galperin, A. L.; Stozhko, N. Y.; Murzakaev, A. M.; Timoshenkova, O. R. *J. Solid State Electrochem.* **2012**, *16*, 2365.
61. Liu, J.; Hurt, A. *Environ. Sci. Technol.* **2010**, *44*, 2169.
62. Hardes, J.; Ahrens, H.; Gebert, C.; Streitberger, A.; Buerger, H.; Erre, M.; Gunsel, A.; Wedemeyer, C.; Saxler, G.; Winkelmann, W.; Gosheger, G. *Biomaterials* **2007**, *28*, 2869.
63. Jovanović, Ž.; Radosavljević, A.; Kačarević-Popović, Z.; Stojkovska, J.; Perić-Grujić, A.; Ristić, M.; Matić, I.; Juranić, Z.; Obradović, B.; Mišković-Stanković, V. *Colloids Surf. B* **2013**, *105*, 230.
64. Wounds International. International Consensus: Appropriate Use of Silver Dressings in Wounds. http://www.woundsinternational.com/clinical-guidelines/international-consensus-appropriate-use-of-silver-dressings-in-wounds (accessed 2012).
65. Kobayashi, M.; Hyu, H. S. *Materials* **2010**, *3*, 2753.
66. Li, F.; Su, Y.; Wang, J.; Wu, G.; Wang, C. *J. Mater. Sci.: Mater. Med.* **2010**, *21*, 147.
67. Kobayashi, M.; Toguchida, J.; Oka, M. K. *Biomaterials.* **2003**, *24*, 639.
68. Baker, M. I.; Walsh, S. P.; Schwartz, Z.; Boyan, B. D. *J. Biomed. Mater. Res. B* **2012**, *100*, 1451.
69. Aydın, R. S. T.; Pulat, M. *J. Nanomater.* **2012** *Article ID 313961*, 1.
70. Khamanga, S. M.; Walker, R. B. *Dissolut. Technol.* **2012**, *3*, 42.
71. Siepmanna, J.; Peppas, N. A. *Int. J. Pharm.* **2011**, *418*, 6.
72. Dash, S.; Murthy, P. N.; Nath, L.; Chowdhury, P. *Acta Polym. Pharm.* **2010**, *67*, 217.
73. Fu, Y.; Kao, W. *J. Expert Opin. Drug Delivery* **2010**, *7*, 429.
74. Bloecker, K.; Englund, M.; Wirth, W.; Hudelmaier, M.; Burgkart, R.; Frobell, R.; Eckstein, F. *BMC Musculoskel. Dis.* **2011**, *12*, 248.
75. Kraus, V. B.; Stabler, T. V.; Kong, S. Y.; Varju, G.; McDaniel, G. *Osteoarthritis Cartilage* **2007**, *15*, 1217.
76. Pencheva, D.; Bryaskova, R.; Kantardjiev, T. *Mater. Sci. Eng.* **2012**, *32*, 2048.